

# Endofullerenes and Dispersion-Corrected Density Functional Approximations: A Cautionary Tale

K. Panchagnula\*<sup>1</sup>, D. Graf<sup>2</sup>, K.R. Bryenton<sup>3</sup>, E.R. Johnson<sup>1,3,4</sup> and A.J.W. Thom<sup>1</sup>

<sup>1</sup>Yusuf Hamied Department of Chemistry, University of Cambridge, Cambridge, United Kingdom

<sup>2</sup>Department of Chemistry, University of Munich (LMU), Munich, Germany

<sup>3</sup>Department of Physics and Atmospheric Science, Dalhousie University, 6310 Coburg Road, Halifax, Nova Scotia, Canada

<sup>4</sup>Department of Chemistry, Dalhousie University, 6243 Alumni Crescent, Halifax, Nova Scotia, Canada

(\*Electronic mail: ksp31@cam.ac.uk)

(Dated: 4 March 2025)

A recent study by Panchagnula *et al.* [J. Chem. Phys. **161**, 054308 (2024)] illustrated the non-concordance of a variety of electronic structure methods at describing the symmetric double-well potential expected along the anisotropic direction of the endofullerene Ne@C<sub>70</sub>. In this article we delve deeper into the difficulties of accurately capturing the dispersion interaction within this system, scrutinising a variety of state-of-the-art density-functional approximations (DFAs) and dispersion corrections (DCs). We identify rigorous criteria for the double-well potential and compare the shapes, barrier heights, and minima positions obtained with the DFAs and DCs to the correlated wavefunction data in the previous study, alongside new coupled-cluster calculations. We show that many of the DFAs are extremely sensitive to the numerical integration grid used, and note that the choice of DC is not independent of the DFA. Functionals with many empirical parameters tuned for main-group thermochemistry do not necessarily result in a reasonable PES, while improved performance can be obtained using nearly dispersionless DFAs with very few empirical parameters and allowing the DC to compensate. We pose the Ne@C<sub>70</sub> system as a challenge to functional developers and as a diagnostic system for testing dispersion corrections, and reiterate the need for more experimental data for comparison.

## I. INTRODUCTION

Non-covalent interactions, particularly London dispersion forces, pose a well-known challenge for *ab initio* electronic structure (ES) methods<sup>1</sup> due to their weak and long-ranged nature. Therefore, chemical species primarily stabilized by dispersion interactions are often difficult to describe accurately with these methods.

Due to its favourable cost-to-performance ratio, density-functional theory (DFT) has earned itself the title of being the “workhorse of quantum chemistry”<sup>2</sup> and has had renowned success across various disciplines. However, its quality is tied to the choice of density-functional approximation (DFA),<sup>3</sup> almost all of which have severe limitations in their ability to accurately capture dispersion interactions. In order to alleviate this, a variety of dispersion corrections (DCs) have been developed,<sup>4</sup> with varying levels of empiricism. These include Grimme’s dispersion corrections,<sup>5–10</sup> as well as the VV10,<sup>11,12</sup> many-body dispersion (MBD),<sup>13,14</sup> and exchange-hole dipole moment (XDM)<sup>15–17</sup> methods. Grimme’s models, in particular, have gained enormous popularity due to their simple and efficient implementation.

Correlated wavefunction (WF) methods are an alternative to DFAs that are reputed for their high accuracy, albeit at the expense of a significant increase in computational cost due to unfavourable scaling with respect to both system and basis-set sizes. As dispersion forces explicitly arise due to the interactions of multiple electrons, WF methods account for this in their description of electron correlation. Second order Møller–Plesset perturbation theory (MP2) is a standout choice due to its efficient implementations,<sup>18–38</sup> whereas coupled cluster (CC) including single, double, and perturbative triple excita-

tions (CCSD(T)) is nominally considered the “gold standard” of WF methods.<sup>39</sup> This impressive level of accuracy comes at a heavy price, as CCSD(T) calculations with moderate basis sets tend to be computationally unfeasible for all but very small chemical systems.

Between the multiple pairings of DFAs and DCs, as well as WF methods, there is a plethora of ES methods that could be used to describe the dispersion interaction within a chemical system. Given an accuracy tolerance, it is not immediately obvious as to which choice can achieve it, and for the lowest computational cost. In order to test, validate, and benchmark ES methods for their ability to describe dispersion interactions accurately and efficiently, endofullerenes (EFs) emerge as interesting candidates.

EFs are a class of systems where atom(s) or molecule(s), A, are trapped within a fullerene cage C<sub>n</sub>, denoted A@C<sub>n</sub>.<sup>40</sup> The development of a technique known as “molecular surgery” has allowed for the controlled synthesis and characterisation of these species, leading to a vast amount of very precise spectroscopic data.<sup>41,42</sup> The sizes of the fullerene rings are such that London dispersion is a significant component of their interaction energies with the encapsulated species. Moreover, they are not too small such that the ES calculations are trivial, and not too large that large basis sets are unfeasible.<sup>43</sup>

Spectroscopic data for these systems probes information about the nuclear energy levels (translational, rotational etc.) of the endohedral species measured at the wavenumber level. In order to achieve this level of accuracy theoretically, the potential energy surface (PES) derived from ES calculations must also be as accurate. However, the development of high level *ab initio* ES techniques is usually focused on the goal of achieving “chemical accuracy” of 1 kcal/mol, which is ap-

proximately 350 cm<sup>-1</sup>. Evidently, requiring the ES methods to move from thermochemical accuracy to spectroscopic accuracy, at the 1 cm<sup>-1</sup> level, significantly increases the computational demand.

A recent theoretical study of He@C<sub>60</sub><sup>44</sup> found that MP2 achieved this level of accuracy, with the random phase approximation (RPA) following closely behind. Experimental data for He@C<sub>60</sub><sup>45,46</sup> was available for comparison, which guided the categorisation of the ES methods, but equivalent data was not present for Ne@C<sub>70</sub>.<sup>47</sup> This larger system proved much more challenging as, even greatly expanding the number and quality of the ES methods considered, a worrying lack of concordance between them was noted. The crux of the difference seemed to lie in the description of the symmetric double well potential along the unique, anisotropic direction of C<sub>70</sub>, with MP2 being a standalone outlier.

In this paper, we delve deeper into the cornucopia of possible ES methods to gain an intuition and understanding of their behaviour for Ne@C<sub>70</sub>. As in our previous work, we investigate a one-dimensional slice of the Ne@C<sub>70</sub> PES along the unique, anisotropic axis of C<sub>70</sub>, and assess its double-well characteristics. We primarily examine the behaviour of various DFAs, as well as different DCs, to understand what properties are important for an accurate description of the endohedral interaction. We compare the characteristics of these PESs to the previously generated correlated WF data, alongside a few new state-of-the-art CC calculations.

## II. THEORY

Previous research on PESs for EFs has tended to forego ES calculations, instead approximating the surface using a pairwise additive Lennard-Jones (LJ) potential, summed over cage-endohedral sites.<sup>48-57</sup> This has the advantage of computational simplicity and ensures that the PES has the appropriate smoothness and symmetry, but at the expense of using empirically derived LJ parameters that may not be optimal.<sup>50,56</sup> On the other hand, due to the high computational cost, generating the full PES from ES calculations requires interpolation between a small set of discrete data points.<sup>47</sup> Therefore, we require the PES obtained from an ES method to be smooth and differentiable.

In the specific case of Ne@C<sub>70</sub>, we expect to see a well-behaved symmetric double well, without any oscillations. More rigorously, we require the origin to be a local maximum, with only two inflection points present. This criterion ensures there are no extra oscillations, nor any shoulders nor plateaus, which could cause failures in the subsequent calculations of vibrational frequencies, intensities, and other derived properties.<sup>58,59</sup> These requirements pose a particular challenge for DFAs, as the energy is usually evaluated on integration grids prone to numerical inaccuracies.<sup>60-68</sup> In the following, we will give a brief summary of the most important aspects of DFT and the associated numerical integration of the energy functionals, while the specific computational details are provided in the supplementary information.

In (Kohn-Sham)-DFT, a system's total energy is given

by<sup>69,70</sup>

$$E_{\text{DFT}} = T_0 + \int v_{\text{ext}}(\mathbf{r})\rho(\mathbf{r})d\mathbf{r} + E_{\text{H}}[\rho] + E_{\text{XC}}, \quad (1)$$

where  $T_0$  is the non-interacting kinetic energy of the electrons,  $v_{\text{ext}}$  is the external potential,  $E_{\text{H}}$  is the Hartree energy, and  $E_{\text{XC}}$  is the exchange-correlation (XC) energy. The XC-energy includes all remaining contributions to the total energy and is hence at the heart of all common DFAs. A large array of different DFAs exists in the literature, with Perdew's ladder<sup>3</sup> providing a classification scheme that groups DFAs into five different "rungs" according to the ingredients used in approximating the XC-energy.

In this work, we employed various DFAs from four of the five rungs and compared their performance on the chosen slice of the Ne@C<sub>70</sub> PES. From rung 2, we employed the generalized gradient approximation (GGA) functional of Perdew-Burke-Ernzerhof (PBE)<sup>71,72</sup> and B86bPBE,<sup>73</sup> which combines Becke's B86b exchange functional with PBE correlation. From rung 3, we picked the combinatorially-optimized meta-GGA (mGGA) including VV10 dispersion from the Head-Gordon group, called B97M-V.<sup>74</sup> From rung 4, we employed hybrid variants of PBE and B86bPBE, termed PBE0<sup>75</sup> and B86bPBE0,<sup>17</sup> with and without various dispersion corrections (*vide infra*). We additionally considered Becke's 10-parameter global hybrid, B97,<sup>76</sup> and the following combinatorially-optimized range-separated hybrids from the Head-Gordon group:  $\omega$ -B97,<sup>77</sup>  $\omega$ -B97X,<sup>77</sup>  $\omega$ -B97X-V,<sup>78</sup> and  $\omega$ -B97M-V.<sup>79</sup> Finally, from rung 5, we chose the double-hybrid B2PLYP<sup>80</sup> and PWPB95<sup>81</sup> functionals from the Grimme group, as well the  $\omega$ -B97M(2)<sup>82</sup> functional from the Head-Gordon group. The functionals used were mainly chosen because of their high popularity and excellent performance in typical benchmarks.<sup>83</sup>

Many XC functionals neglect the energy contribution from dispersion effects, so a correction term must be added. Usually, the contribution of dispersion to the electron density is negligible; therefore, a popular approach is to include dispersion as a post-self-consistent-field (post-SCF) correction to the total DFT energy as

$$E_{\text{Total}} = E_{\text{DFT}} + E_{\text{disp}}. \quad (2)$$

Various post-SCF dispersion correction methods have been developed that depend on different system properties. For instance, the Grimme DFT-D series, such as D3(0)<sup>6</sup> and D3(BJ),<sup>84</sup> depend on coordination number. The term in parentheses indicates the specific damping function applied to the DC, ensuring appropriate asymptotic behaviour by making the dispersion energy become constant at small internuclear separations. These functions contain tunable parameters that are optimised for each functional and sometimes basis set. D3(0) and D3(BJ) use the Chai and Head-Gordon<sup>85</sup> and Becke-Johnson (BJ)<sup>86</sup> damping functions, respectively. The Tkatchenko-Scheffler (TS)<sup>87</sup> and many-body dispersion (MBD)-based models, such as the range-separated self-consistent screening (MBD@rsSCS)<sup>13,88</sup> and non-local (MBD-NL)<sup>14</sup> variants, depend on the electron density and use Fermi-type Wu-Yang damping functions.<sup>89</sup> The XDM

model<sup>16,17,90</sup> depends not only on the density, but also its gradient, Laplacian, and the kinetic-energy density, and uses the BJ damping function.

In this work, we considered the PBE0 hybrid functional paired with each of the D3(0), D3(BJ), TS, MBD@rsSCS, MBD-NL, and XDM dispersion methods. XDM was also paired with the B86bPBE0 hybrid as B86b is better able to describe non-bonded repulsion, as a result of the adherence of its enhancement factor to the appropriate large reduced-density-gradient limit.<sup>91</sup> As the mixing parameters for the MP2 contribution in the B2PLYP and PWPB95 double-hybrid functionals are smaller than unity, they were combined with D3(BJ) to ensure an asymptotically correct description of long-range dispersion effects.<sup>81,92</sup> Note that the B97M-V,  $\omega$ -B97X-V,  $\omega$ -B97M-V, and  $\omega$ -B97M(2) functionals were not paired with another dispersion correction as they already include the VV10 dispersion method in their definitions. While  $\omega$ -B97X does not include a dispersion correction, it was parameterized to reference data involving dispersion-bound systems and, therefore, captures some short-range dispersion-like binding through its exchange terms.

Although the chosen DFAs exhibit significantly different functional forms, they share the common characteristic that their energies are evaluated on a numerical integration grid. Typically, the molecular grid is decomposed into a collection of atom-centered grids using Becke’s partitioning<sup>93</sup> or other similar schemes.<sup>94,95</sup> Each atomic grid is generally constructed as a product of radial and angular grids, denoted as a tuple of (radial points, angular points) used, with the angular points corresponding to the Lebedev quadratures.<sup>96</sup> The behaviour of functionals for intermolecular interactions can be extremely sensitive to the integration grid. Too small a grid can not only mean that certain integrals do not converge, but in the case of certain DFAs, introduce spurious oscillations into the PES, essentially rendering it useless.<sup>58–67</sup> On the other hand, too large a grid can severely increase the computational cost, making the calculation infeasible. The sensitivity of the computed Ne@C<sub>70</sub> PES to the integration grid is illustrated in the SI for the case of  $\omega$ -B97M-V and, without extremely dense angular integration grids, the PES obtained with certain functionals exhibited strong oscillations.

### III. RESULTS

In Figure 1a, complete basis set (CBS) extrapolated correlated wavefunction data for the MP2 (blue) and RPA@PBE (orange) from our previous study are reproduced.<sup>47</sup> The MP2 curve represents the extreme of the WF data obtained previously, giving the most binding, while RPA@PBE is an intermediate result. The green scatter points are new data from the present work derived from paired natural orbital (PNO) CCSD(T0) calculations, also extrapolated to both the complete PNO space and CBS limit.<sup>97</sup> (T0) refers to a quasi-canonical implementation of the perturbative triples, a consequence of using PNOs.<sup>98</sup> Two metrics that will be used to describe the overall shape of the PES are the minima positions ( $z_m$ , in Å) and the barrier height (BH, in cm<sup>-1</sup>) connect-

TABLE I: Barrier heights and minima positions for different DFAs and WF methods in Figure 1.

Method	BH/cm <sup>-1</sup>	$z_m/\text{Å}$
HF	0	0
PBE	0	0
B97	0	0
$\omega$ -B97X	33.48	0.58
B97M-V	114.64	0.86
$\omega$ -B97X-V	59.94	0.68
$\omega$ -B97M-V	64.71	0.82
B2PLYP-D3(BJ)	61.85	0.78
PWPB95-D3(BJ)	293.43	0.74
$\omega$ -B97M(2)	89.84	0.74
MP2	84.21	0.76
RPA@PBE	35.43	0.64
PNO-CCSD(T0) <sup>†</sup>	≥ 36.1	-

<sup>†</sup> S.P. calculation at  $z = 0.50$  represents the BH lower bound

ing them; the magnitude of the BH exactly corresponds to the well depth since the zero of energy is defined to be the point at  $z = 0$  with the Ne at the centre of the C<sub>70</sub> cage. The new CCSD(T0) data suggests that the true BH and  $z_m$  are likely to lie between the values predicted by MP2 and RPA@PBE, and this should serve as a reference when considering the results of the various DFAs.

Figure 1b shows results for the Ne@C<sub>70</sub> PES obtained with the selected GGAs and GGA-based hybrids (solid lines), mGGA-based hybrids (dashed lines), and double hybrids (dotted lines). Table I further summarises the obtained minima positions and barrier heights with selected methods. The dispersion-uncorrected methods (HF, PBE, and B97) expectedly display only a single well while the remaining methods all display double wells, but of varying characters. The mGGA-based hybrids (B97M-V and  $\omega$ -B97M-V) exhibit wider double wells with higher values of  $z_m$  than their analogous GGA-based hybrids ( $\omega$ -B97X and  $\omega$ -B97X-V) or obtained with WF methods, indicating they are likely erroneous. Additionally, the  $\omega$ B97M(2), B97M-V, and PWPB95-D3(BJ) curves exhibit even deeper double wells than obtained with MP2, with the PWPB95-D3(BJ) double hybrid being a severe outlier with a barrier of nearly 300 cm<sup>-1</sup>. This latter PES also shows some very subtle wiggles, which is likely caused by the high sensitivity of the underlying B95 mGGA to grid size.<sup>15,61</sup> The functionals providing PES with the most comparable features to the WF results are  $\omega$ -B97X, followed by  $\omega$ -B97X-V and B2PLYP-D3(BJ), although the predicted BH and  $z_m$  values still vary significantly amongst this group. The good performance of  $\omega$ -B97X here is surprising as it does not include an explicit dispersion-energy term. Given the large spread in the computed results, we suggest that functionals that contain many parameters, and are traditionally designed for thermochemistry, may not perform well for this PES.

Next, we turn our attention to minimally empirical functionals designed for intermolecular interactions. In Figure 2, we consider PBE0 as the base functional to which an assortment of different DCs (XDM, TS, MBD-NL, MBD@rsSCS, D3(0), and D3(BJ)) are added as described in Eq (2). PBE0

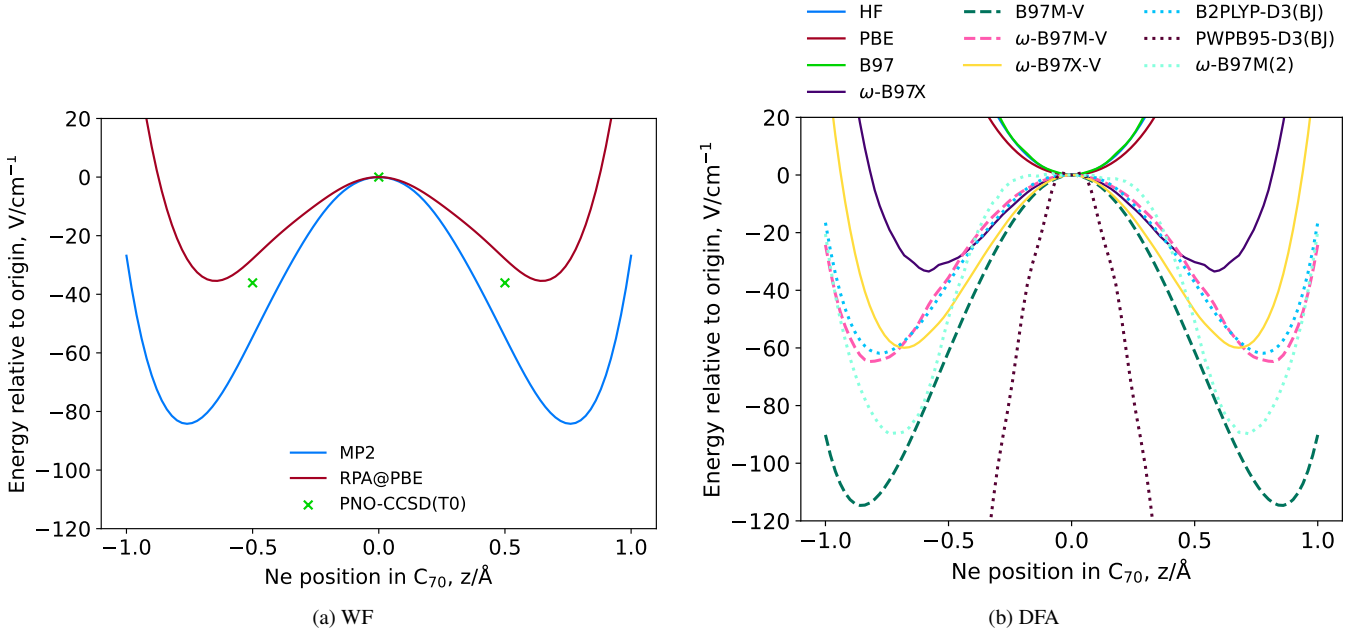


FIG. 1: PES slices of (a) WF methods and (b) DFAs for points separated by  $0.02\text{\AA}$ . For the WF methods, MP2 is shown in blue and RPA@PBE in maroon; PNO-CCSD(T0) single points are given by the light green crosses. For the DFAs, GGAs and GGA-based hybrids are given by solid lines, mGGA-based hybrids by dashed lines, and double hybrids by dotted lines. HF, PBE, B97,  $\omega$ -B97X, B97M-V,  $\omega$ -B97M-V,  $\omega$ -B97X-V, B2PLYP-D3(BJ), PWPB95-D3(BJ),  $\omega$ -B97M(2) are in blue, maroon, light green, purple, forest green, pink, yellow, light blue, brown and turquoise.

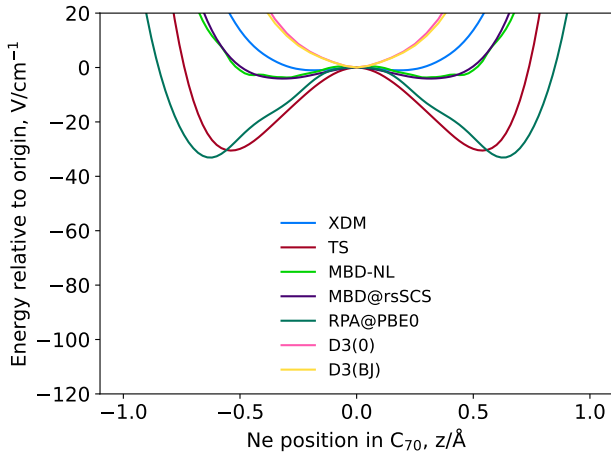


FIG. 2: PES slices of PBE0 with dispersion corrections XDM, TS, MBD-NL, MBD@rsSCS, D3(0), D3(BJ) in blue, maroon, light green, purple, pink and yellow. RPA@PBE0, a correlated WF method, is in forest green.

is chosen as corresponding damping parameters are readily available for each of these DCs. Both D3-type corrections exhibit a single minimum, indicating that they are not capturing sufficient information about the strength of dispersion interaction to transform the PBE0 curve (which also has a single minimum) into a double well. Furthermore, the XDM, MBD-NL,

and MBD@rsSCS curves display extremely flat double wells, with BHs of  $<5\text{ cm}^{-1}$ , much smaller than what was previously observed from the correlated wavefunction data in Figure 1a. On the other hand, PBE0-TS yields a BH of  $30.5\text{ cm}^{-1}$  and minima at  $z_m = \pm 0.54\text{ \AA}$ , in line with the RPA@PBE0 results. This increased well depth, relative to the other DCs, is in keeping with the tendency of TS to overbind in comparison to the other DCs when benchmarked for intermolecular complexes and molecular crystals.<sup>17</sup>

The ability of PBE0-TS to capture the double well may be a consequence of how the zero of energy is defined relative to Ne at the centre of the C<sub>70</sub>, and there being dispersion contributions from both sides of the fullerene cage. It is important to realise that we are most interested in how the dispersion energy *changes* as the PES is traversed,<sup>68</sup> not just its absolute value, which will be relatively large as this is the major component of the binding of noble gas endofullerenes. While the TS approach would likely overestimate the magnitude of the absolute binding energy relative to infinitely separated Ne and C<sub>70</sub>, the increased magnitude of the TS dispersion term improves the description of the double well when paired with PBE0.

While it may seem possible to choose any base functional, and subsequently pair it with any DC, these choices are not necessarily independent. There is a subtle interplay between these quantities that is reflected by the sensitivity of the empirical damping parameters on the choice of base functional. These parameters are present in all post-SCF dispersion meth-

TABLE II: Barrier heights and minima positions for different dispersion corrections applied to PBE0 and B86bPBE0 calculations in Figures 2 and 3.

Method	BH/cm <sup>-1</sup>	$z_m/\text{\AA}$
PBE0-XDM	1.02	0.18
PBE0-TS	30.54	0.54
PBE0-MBD-NL	3.67	0.30
PBE0-MBD@rsSCS	4.07	0.32
PBE0-D3(0)	0	0
PBE0-D3(BJ)	0	0
B86bPBE0-XDM	10.91	0.44
B86bPBE0-50X-XDM	27.44	0.56
B86bPBE0-50X-XDM(BJ <sub>NG</sub> ) <sup>†</sup>	36.59	0.60
RPA@PBE0	33.10	0.62

<sup>†</sup> BJ damping fit to noble gases ( $a_1 = 0.65$  &  $a_2 = 1.68 \text{\AA}$ )<sup>100</sup>

ods to damp the dispersion energy at short interatomic separations, and are fit for each choice of base functional using reference WF data for molecular complexes. This implies that, as the base functional captures a better description of non-bonded repulsion, the less the DC needs to be damped. Conversely, the dispersion term is more damped when paired with functionals that already mimic some dispersion-like binding through their exchange terms, or include a fraction of MP2 correlation as in double hybrids. Damping parameter optimization is further complicated as the reference data is not typically limited to only dispersion-bound systems and spans a broad range of intermolecular interaction types, including hydrogen bonding. This results in error cancellation between delocalisation error in the base functional<sup>99</sup> and the DC in some cases, particularly for GGAs.

Finally, we examine the importance of the choice of base density functional, and the specific fraction of exact-exchange (HF) mixing,  $a_X$ , for sequences of hybrid functionals based on PBE0 and B86bPBE0. The  $a_X$  parameter was varied in increments of 5% from 0% to 50% exact exchange as higher mixing fractions tend to lead to deleterious performance for main-group thermochemistry due to the mismatch between non-local exchange and local correlation functionals.<sup>101</sup> The computed BHs and  $z_m$  for the Ne@C<sub>70</sub> PES are plotted as a function of  $a_X$  in Figs 3a and 3b, respectively, for these functionals with (crosses) and without (circles) XDM dispersion included. This allows for scrutinisation of the interplay of the base functional and dispersion correction, and exploration into an optimal value(s) for the precise amount of HF exchange. As XDM is fitted to each functional and basis set combination, the BJ damping coefficients ( $a_1$  and  $a_2$ ) needed re-optimization for each value of  $a_X$  considered. Further discussion, tables of optimal coefficients, and PES plots are provided in the SI.

For this particular PES, there is very little difference in the results obtained with the PBE-based and B86b-based hybrid functionals without a DC. This occurs because we are only sampling the PES for translation of Ne inside the C<sub>70</sub> cage. The primary difference between these exchange functionals is for regions far from atoms or molecules, where the electron density is decaying exponentially and the reduced density

gradient is large, but no such regions are present within end-ofullerenes. There is, however, some dependence of the PES on the degree of exact-exchange mixing. As seen in Fig. 3, the GGA functionals ( $a_X = 0$ ) predict only a single well, but this transitions to a shallow double well with BHs of ca. 1-8 cm<sup>-1</sup> as  $a_X$  is increased beyond 25% exact exchange. The softening of the potential with increased exact-exchange mixing implies that both GGA exchange functionals are too repulsive for this potential, compared to Hartree-Fock.

In contrast, there are significant differences between the PES predicted by the PBE-based and B86b-based hybrids when the XDM dispersion correction is included. As seen in Fig. 3, the hybrids based on B86bPBE0-XDM always exhibit a double well, with both the BHs and  $z_m$ s increasing nearly linearly (between 2–27 cm<sup>-1</sup> and 0.35–0.55 Å respectively) with increasing  $a_X$ . This effect is also seen for the hybrid functionals based on PBE0-XDM, but to a much lesser extent, so that the double well only appears beyond 20% HF exchange. The reasons for the deeper double wells seen with functionals based on B86bPBE0-XDM, compared to PBE0-XDM, can be traced to the interplay between the base functional and the dispersion damping function. Generally, PBE0 tends to give more binding for intermolecular complexes than B86bPBE0, so the PBE0 DC from XDM is more damped. Further, as  $a_X$  is increased, the binding energies for intermolecular complexes (particularly hydrogen-bonded complexes) decrease in magnitude, so the DC is less damped. This means that the magnitude of the dispersion energies will increase both upon changing from PBE0-XDM to B86bPBE0-XDM, and with increasing  $a_X$ , as reflected in the computed BH and  $z_m$  values in Fig. 3.

In general, an accurate base functional should be dispersionless and have minimal delocalisation error, to allow the DC to do the heavy lifting.<sup>91</sup> These requirements are best met by B86bPBE0-XDM with 50% exact exchange, which has the best match with the previous correlated wavefunction data<sup>47</sup> of the functionals considered in Fig. 3. It is likely that even deeper wells would be obtained for exact-exchange mixing fractions of greater than 50%, although such functionals would not be recommended for general thermochemistry. It is interesting to note that, if XDM’s BJ damping function uses parameters that are fit for noble gases rather than molecular dimers,<sup>100</sup> then the double well deepens somewhat further. For B86bPBE0-50x-XDM, the BH deepens from 27.44 to 36.59 cm<sup>-1</sup>, and  $z_m$  extends from  $\pm 0.54$  to  $\pm 0.60$  Å, leading to improved agreement with the RPA@PBE0 and the PNO-CCSD(T0) results, as shown in Table II.

#### IV. CONCLUSION

In this paper, we have investigated the behaviour of a variety of functionals, as well as dispersion corrections at describing the symmetric double-well potential in the Ne@C<sub>70</sub> endo-fullerene along its unique, anisotropic direction. This system was chosen due to its challenging nature for a concordant description of its PES between a variety of both WF and DFA methods. Through our exploration of different DFAs, span-

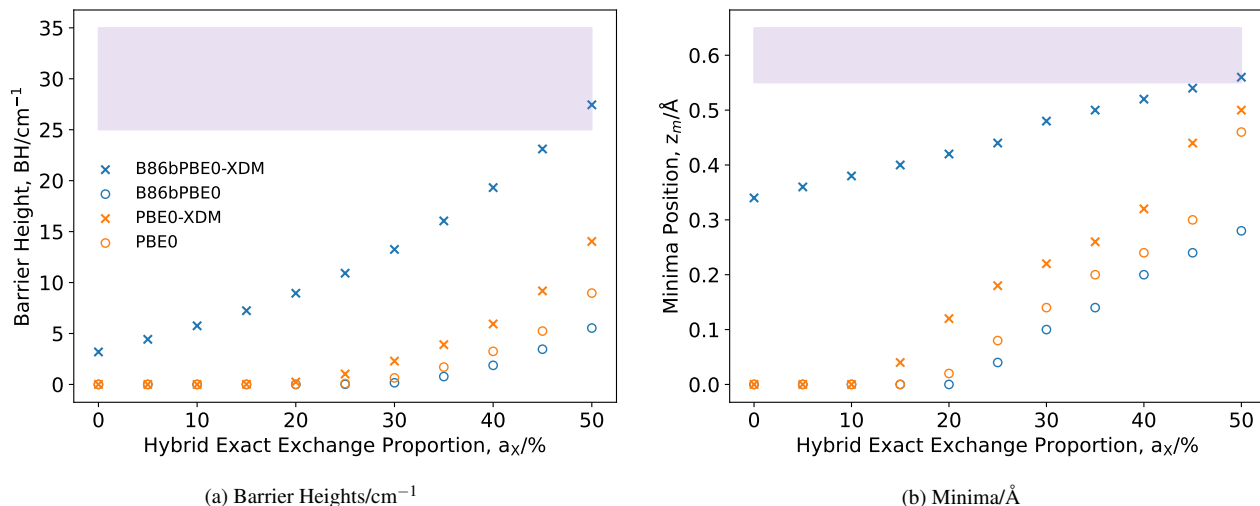


FIG. 3: Double well features (a) BH and (b)  $z_m$  for B86bPBE0 (blue) and PBE0 (maroon) with (crosses) and without (circles) XDM dispersion for varying exact HF exchange proportion. The shaded purple regions span the range of WF data obtained from the previous study that are in the best agreement with the PNO-CCSD(T0) results.

ning through most rungs of Perdew’s ladder, it is apparent that the choice of base functional, and corresponding integration grid, is crucial. It is not the case that a higher rung functional necessarily performs better, but the more fitted parameters the functional includes, the more sensitive it tends to be. The choice of dispersion correction is also an important one, with a range of barrier heights and minima positions possible depending on the specific choice. This is also affected by the choice of base functional, due to the interplay of the damping term between the functional and correction. When considering hybrid functionals, the precise amount of HF exchange is also a key variable, due to both the composition of the data sets used to fit the functional-dependent dispersion damping parameters and the functionals’ ability to describe non-bonded repulsion in Ne@C<sub>70</sub>.

Overall, the Ne@C<sub>70</sub> system is extremely challenging for current state-of-the-art ES methods. As shown, almost any BH and  $z_m$  can be calculated, depending on the particular DFA and DC, with very few combinations falling in the previously attributed low and middle BH regimes. From the DFT perspective, it may be a leap too far to expect accurate and concordant results when even the WF methods are not in agreement with themselves. However, we can conclude that it is extremely important to use a base functional that obeys the physics of the system with as few empirically derived factors as possible. Functionals developed with only thermochemistry in mind are not well suited for a good description of the PES. It may be more pertinent to choose a base functional that is dispersionless, allowing for calculation of the correlation energy using virtual orbitals (as in double hybrid functionals) and/or an added dispersion correction.

We recommend Ne@C<sub>70</sub> as a diagnostic system to test correlation methods or dispersion corrections when developing new cutting-edge DFT methods. We also call for more experimental data on this system, in order to further drive improve-

ment of electronic structure methods.

## SUPPLEMENTARY INFORMATION

See the Supplementary Information for more precise computational details for all the DFAs and WF methods shown, alongside some more detailed plots of the hybrid functional PES slices.

## ACKNOWLEDGMENTS

KRB and ERJ thank the Natural Sciences and Engineering Research Council (NSERC) of Canada for financial support and the Atlantic Computing Excellence Network (ACENET) for computational resources. ERJ also thanks the Royal Society for a Wolfson Visiting Fellowship. DG acknowledges funding by the Deutsche Forschungsgemeinschaft (DFG, German Research Foundation) – 498448112. DG thanks J. Kussmann (LMU Munich) for providing a development version of the FermiONs++ software package. DG further thanks H. Laqua (UC Berkeley) for helpful discussions. KP would like to thank David Tew for providing the CCSD(T0) data alongside a brief explanation of the method and its consequences.

<sup>1</sup>S. Grimme, A. Hansen, J. G. Brandenburg, and C. Bannwarth, “Dispersion-Corrected Mean-Field Electronic Structure Methods,” *Chemical Reviews* **116**, 5105–5154 (2016).

<sup>2</sup>A. M. Teale, T. Helgaker, A. Savin, C. Adamo, B. Aradi, A. V. Arbuznikov, P. W. Ayers, E. J. Baerends, V. Barone, P. Calaminici, E. Cancès, E. A. Carter, P. K. Chattaraj, H. Chermette, I. Ciofini, T. D. Crawford, F. D. Proft, J. F. Dobson, C. Draxl, T. Frauenheim, E. Fromager, P. Fuentealba, L. Gagliardi, G. Galli, J. Gao, P. Geerlings, N. Gidopoulos, P. M. W. Gill, P. Gori-Giorgi, A. Görling, T. Gould, S. Grimme, O. Gritsenko, H. J. A.

- Jensen, E. R. Johnson, R. O. Jones, M. Kaupp, A. M. Köster, L. Kronik, A. I. Krylov, S. Kvaal, A. Laestadius, M. Levy, M. Lewin, S. Liu, P.-F. Loos, N. T. Maitra, F. Neese, J. P. Perdew, K. Pernal, P. Pernot, P. Piecuch, E. Rebolini, L. Reining, P. Romaniello, A. Ruzsinszky, D. R. Salahub, M. Scheffler, P. Schwerdtfeger, V. N. Staroverov, J. Sun, E. Tellgren, D. J. Tozer, S. B. Trickey, C. A. Ullrich, A. Vela, G. Vignale, T. A. Wesolowski, X. Xu, and W. Yang, "DFT exchange: Sharing perspectives on the workhorse of quantum chemistry and materials science," *Physical Chemistry Chemical Physics* **24**, 28700–28781 (2022).
- <sup>3</sup>J. P. Perdew and K. Schmidt, "Jacob's ladder of density functional approximations for the exchange-correlation energy," *AIP Conference Proceedings* **577**, 1–20 (2001).
- <sup>4</sup>J. Klimeš and A. Michaelides, "Perspective: Advances and challenges in treating van der Waals dispersion forces in density functional theory," *The Journal of Chemical Physics* **137**, 120901 (2012).
- <sup>5</sup>S. Grimme, "Accurate description of van der Waals complexes by density functional theory including empirical corrections," *Journal of Computational Chemistry* **25**, 1463–1473 (2004).
- <sup>6</sup>S. Grimme, J. Antony, S. Ehrlich, and H. Krieg, "A consistent and accurate ab initio parametrization of density functional dispersion correction (DFT-D) for the 94 elements H-Pu," *The Journal of Chemical Physics* **132**, 154104 (2010).
- <sup>7</sup>S. Grimme, "Improved second-order Møller–Plesset perturbation theory by separate scaling of parallel- and antiparallel-spin pair correlation energies," *The Journal of Chemical Physics* **118**, 9095–9102 (2003).
- <sup>8</sup>S. Grimme, "Semiempirical GGA-type density functional constructed with a long-range dispersion correction," *Journal of Computational Chemistry* **27**, 1787–1799 (2006).
- <sup>9</sup>E. Caldeweyher, C. Bannwarth, and S. Grimme, "Extension of the D3 dispersion coefficient model," *The Journal of Chemical Physics* **147**, 034112 (2017).
- <sup>10</sup>E. Caldeweyher, S. Ehlert, A. Hansen, H. Neugebauer, S. Spicher, C. Bannwarth, and S. Grimme, "A generally applicable atomic-charge dependent London dispersion correction," *The Journal of Chemical Physics* **150**, 154122 (2019).
- <sup>11</sup>O. A. Vydrov and T. Van Voorhis, "Nonlocal van der Waals density functional: The simpler the better," *The Journal of Chemical Physics* **133**, 244103 (2010).
- <sup>12</sup>R. Sabatini, T. Gorni, and S. de Gironcoli, "Nonlocal van der Waals density functional made simple and efficient," *Physical Review B* **87**, 041108 (2013).
- <sup>13</sup>A. Ambrosetti, A. M. Reilly, R. A. DiStasio, Jr., and A. Tkatchenko, "Long-range correlation energy calculated from coupled atomic response functions," *The Journal of Chemical Physics* **140**, 18A508 (2014).
- <sup>14</sup>J. Hermann and A. Tkatchenko, "Density Functional Model for van der Waals Interactions: Unifying Many-Body Atomic Approaches with Non-local Functionals," *Physical Review Letters* **124**, 146401 (2020).
- <sup>15</sup>E. R. Johnson and A. D. Becke, "A post-Hartree–Fock model of intermolecular interactions," *The Journal of Chemical Physics* **123**, 024101 (2005).
- <sup>16</sup>A. D. Becke and E. R. Johnson, "Exchange-hole dipole moment and the dispersion interaction revisited," *The Journal of Chemical Physics* **127**, 154108 (2007).
- <sup>17</sup>A. J. A. Price, A. Otero-de-la-Roza, and E. R. Johnson, "XDM-corrected hybrid DFT with numerical atomic orbitals predicts molecular crystal lattice energies with unprecedented accuracy," *Chemical Science* **14**, 1252–1262 (2023).
- <sup>18</sup>P. Pulay, "Localizability of dynamic electron correlation," *Chemical Physics Letters* **100**, 151–154 (1983).
- <sup>19</sup>M. Häser, "Møller–Plesset (MP2) perturbation theory for large molecules," *Theoretica chimica acta* **87**, 147–173 (1993).
- <sup>20</sup>P. E. Maslen and M. Head-Gordon, "Non-iterative local second order Møller–Plesset theory," *Chemical Physics Letters* **283**, 102–108 (1998).
- <sup>21</sup>P. Y. Ayala and G. E. Scuseria, "Linear scaling second-order Møller–Plesset theory in the atomic orbital basis for large molecular systems," *The Journal of Chemical Physics* **110**, 3660–3671 (1999).
- <sup>22</sup>M. Schütz, G. Hetzer, and H.-J. Werner, "Low-order scaling local electron correlation methods. I. Linear scaling local MP2," *The Journal of Chemical Physics* **111**, 5691–5705 (1999).
- <sup>23</sup>S. Saebø and P. Pulay, "A low-scaling method for second order Møller–Plesset calculations," *The Journal of Chemical Physics* **115**, 3975–3983 (2001).
- <sup>24</sup>H.-J. Werner, F. R. Manby, and P. J. Knowles, "Fast linear scaling second-order Møller–Plesset perturbation theory (MP2) using local and density fitting approximations," *The Journal of Chemical Physics* **118**, 8149–8160 (2003).
- <sup>25</sup>Y. Jung and M. Head-Gordon, "A fast correlated electronic structure method for computing interaction energies of large van der Waals complexes applied to the fullerene–porphyrin dimer," *Physical Chemistry Chemical Physics* **8**, 2831–2840 (2006).
- <sup>26</sup>Y. Jung, Y. Shao, and M. Head-Gordon, "Fast evaluation of scaled opposite spin second-order Møller–Plesset correlation energies using auxiliary basis expansions and exploiting sparsity," *Journal of Computational Chemistry* **28**, 1953–1964 (2007).
- <sup>27</sup>B. Doser, D. S. Lambrecht, and C. Ochsenfeld, "Tighter multipole-based integral estimates and parallel implementation of linear-scaling AO–MP2 theory," *Physical Chemistry Chemical Physics* **10**, 3335–3344 (2008).
- <sup>28</sup>B. Doser, D. S. Lambrecht, J. Kussmann, and C. Ochsenfeld, "Linear-scaling atomic orbital-based second-order Møller–Plesset perturbation theory by rigorous integral screening criteria," *The Journal of Chemical Physics* **130**, 064107 (2009).
- <sup>29</sup>J. Zienau, L. Clin, B. Doser, and C. Ochsenfeld, "Cholesky-decomposed densities in Laplace-based second-order Møller–Plesset perturbation theory," *The Journal of Chemical Physics* **130**, 204112 (2009).
- <sup>30</sup>K. Kristensen, I.-M. Høyvik, B. Jansik, P. Jørgensen, T. Kjærgaard, S. Reine, and J. Jakowski, "MP2 energy and density for large molecular systems with internal error control using the Divide-Expand-Consolidate scheme," *Physical Chemistry Chemical Physics* **14**, 15706–15714 (2012).
- <sup>31</sup>S. A. Maurer, L. Clin, and C. Ochsenfeld, "Cholesky-decomposed density MP2 with density fitting: Accurate MP2 and double-hybrid DFT energies for large systems," *The Journal of Chemical Physics* **140**, 224112 (2014).
- <sup>32</sup>P. Pinski, C. Riplinger, E. F. Valeev, and F. Neese, "Sparse maps—A systematic infrastructure for reduced-scaling electronic structure methods. I. An efficient and simple linear scaling local MP2 method that uses an intermediate basis of pair natural orbitals," *The Journal of Chemical Physics* **143**, 034108 (2015).
- <sup>33</sup>P. R. Nagy, G. Samu, and M. Kállay, "An Integral-Direct Linear-Scaling Second-Order Møller–Plesset Approach," *Journal of Chemical Theory and Computation* **12**, 4897–4914 (2016).
- <sup>34</sup>P. Baudin, P. Ettenhuber, S. Reine, K. Kristensen, and T. Kjærgaard, "Efficient linear-scaling second-order Møller–Plesset perturbation theory: The divide–expand–consolidate RI-MP2 model," *The Journal of Chemical Physics* **144**, 054102 (2016).
- <sup>35</sup>B. Q. Pham and M. S. Gordon, "Hybrid Distributed/Shared Memory Model for the RI-MP2 Method in the Fragment Molecular Orbital Framework," *Journal of Chemical Theory and Computation* **15**, 5252–5258 (2019).
- <sup>36</sup>G. M. J. Barca, S. C. McKenzie, N. J. Bloomfield, A. T. B. Gilbert, and P. M. W. Gill, "Q-MP2-OS: Møller–Plesset Correlation Energy by Quadrature," *Journal of Chemical Theory and Computation* **16**, 1568–1577 (2020).
- <sup>37</sup>M. Glasbrenner, D. Graf, and C. Ochsenfeld, "Efficient Reduced-Scaling Second-Order Møller–Plesset Perturbation Theory with Cholesky-Decomposed Densities and an Attenuated Coulomb Metric," *Journal of Chemical Theory and Computation* **16**, 6856–6868 (2020).
- <sup>38</sup>A. Förster, M. Franchini, E. van Lenthe, and L. Visscher, "A Quadratic Pair Atomic Resolution of the Identity Based SOS-AO-MP2 Algorithm Using Slater Type Orbitals," *Journal of Chemical Theory and Computation* **16**, 875–891 (2020).
- <sup>39</sup>P. R. Nagy, "State-of-the-art local correlation methods enable affordable gold standard quantum chemistry for up to hundreds of atoms," *Chemical Science* **15**, 14556–14584 (2024).
- <sup>40</sup>Z. Bačić, "Perspective: Accurate treatment of the quantum dynamics of light molecules inside fullerene cages: Translation-rotation states, spectroscopy, and symmetry breaking," *The Journal of Chemical Physics* **149**, 100901 (2018).
- <sup>41</sup>S. Bloodworth and R. J. Whitby, "Synthesis of endohedral fullerenes by molecular surgery," *Communications Chemistry* **5**, 1–14 (2022).

- <sup>42</sup>M. H. Levitt, "Spectroscopy of light-molecule endofullerenes," *Philosophical Transactions of the Royal Society A: Mathematical, Physical and Engineering Sciences* **371**, 20120429 (2013).
- <sup>43</sup>J. Cioslowski, "Electronic Structure Calculations on Endohedral Complexes of Fullerenes: Reminiscences and Prospects," *Molecules* **28**, 1384 (2023).
- <sup>44</sup>K. Panchagnula, D. Graf, F. E. A. Albertani, and A. J. W. Thom, "Translational eigenstates of He@C60 from four-dimensional ab initio potential energy surfaces interpolated using Gaussian process regression," *The Journal of Chemical Physics* **160**, 104303 (2024).
- <sup>45</sup>G. R. Bacanu, T. Jafari, M. Aouane, J. Rantaharju, M. Walkey, G. Hoffman, A. Shugai, U. Nagel, M. Jiménez-Ruiz, A. J. Horsewill, S. Rols, T. Rööm, R. J. Whitby, and M. H. Levitt, "Experimental determination of the interaction potential between a helium atom and the interior surface of a C60 fullerene molecule," *The Journal of Chemical Physics* **155**, 144302 (2021).
- <sup>46</sup>T. Jafari, G. R. Bacanu, A. Shugai, U. Nagel, M. Walkey, G. Hoffman, M. H. Levitt, R. J. Whitby, and T. Rööm, "Terahertz spectroscopy of the helium endofullerene He@C60," *Physical Chemistry Chemical Physics* **24**, 9943–9952 (2022).
- <sup>47</sup>K. Panchagnula, D. Graf, E. R. Johnson, and A. J. W. Thom, "Targeting spectroscopic accuracy for dispersion bound systems from ab initio techniques: Translational eigenstates of Ne@C70," *The Journal of Chemical Physics* **161**, 054308 (2024).
- <sup>48</sup>M. Xu, F. Sebastianelli, Z. Bačić, R. Lawler, and N. J. Turro, "H<sub>2</sub>, HD, and D<sub>2</sub> inside C60: Coupled translation-rotation eigenstates of the endohedral molecules from quantum five-dimensional calculations," *The Journal of Chemical Physics* **129**, 064313 (2008).
- <sup>49</sup>M. Xu, F. Sebastianelli, Z. Bačić, R. Lawler, and N. J. Turro, "Quantum dynamics of coupled translational and rotational motions of H<sub>2</sub> inside C60," *The Journal of Chemical Physics* **128**, 011101 (2008).
- <sup>50</sup>M. Xu, F. Sebastianelli, B. R. Gibbons, Z. Bačić, R. Lawler, and N. J. Turro, "Coupled translation-rotation eigenstates of H<sub>2</sub> in C60 and C70 on the spectroscopically optimized interaction potential: Effects of cage anisotropy on the energy level structure and assignments," *The Journal of Chemical Physics* **130**, 224306 (2009).
- <sup>51</sup>M. Xu, S. Ye, A. Powers, R. Lawler, N. J. Turro, and Z. Bačić, "Inelastic neutron scattering spectrum of H<sub>2</sub>@C60 and its temperature dependence decoded using rigorous quantum calculations and a new selection rule," *The Journal of Chemical Physics* **139**, 064309 (2013).
- <sup>52</sup>P. M. Felker and Z. Bačić, "Communication: Quantum six-dimensional calculations of the coupled translation-rotation eigenstates of H<sub>2</sub>O@C60," *The Journal of Chemical Physics* **144**, 201101 (2016).
- <sup>53</sup>M. Xu, P. M. Felker, and Z. Bačić, "Light molecules inside the nanocavities of fullerenes and clathrate hydrates: Inelastic neutron scattering spectra and the unexpected selection rule from rigorous quantum simulations," *International Reviews in Physical Chemistry* **39**, 425–463 (2020).
- <sup>54</sup>P. M. Felker and Z. Bačić, "Flexible water molecule in C60: Intramolecular vibrational frequencies and translation-rotation eigenstates from fully coupled nine-dimensional quantum calculations with small basis sets," *The Journal of Chemical Physics* **152**, 014108 (2020).
- <sup>55</sup>T. Jafari, A. Shugai, U. Nagel, G. R. Bacanu, M. Aouane, M. Jiménez-Ruiz, S. Rols, S. Bloodworth, M. Walkey, G. Hoffman, R. J. Whitby, M. H. Levitt, and T. Rööm, "Ne, Ar, and Kr oscillators in the molecular cavity of fullerene C60," *The Journal of Chemical Physics* **158**, 234305 (2023).
- <sup>56</sup>K. Panchagnula and A. J. W. Thom, "Exploring the parameter space of an endohedral atom in a cylindrical cavity," *The Journal of Chemical Physics* **159**, 164308 (2023).
- <sup>57</sup>M. Mandziuk and Z. Bačić, "Quantum three-dimensional calculation of endohedral vibrational levels of atoms inside strongly nonspherical fullerenes: Ne@C70," *The Journal of Chemical Physics* **101**, 2126–2140 (1994).
- <sup>58</sup>S. P. Sitkiewicz, R. Zaleśny, E. Ramos-Cordoba, J. M. Luis, and E. Matito, "How Reliable Are Modern Density Functional Approximations to Simulate Vibrational Spectroscopies?" *The Journal of Physical Chemistry Letters* **13**, 5963–5968 (2022).
- <sup>59</sup>S. P. Sitkiewicz, R. R. Ferradás, E. Ramos-Cordoba, R. Zaleśny, E. Matito, and J. M. Luis, "Spurious Oscillations Caused by Density Functional Approximations: Who is to Blame? Exchange or Correlation?" *Journal of Chemical Theory and Computation* **20**, 3144–3153 (2024).
- <sup>60</sup>E. R. Johnson, R. A. Wolkow, and G. A. DiLabio, "Application of 25 density functionals to dispersion-bound homomolecular dimers," *Chemical Physics Letters* **394**, 334–338 (2004).
- <sup>61</sup>E. R. Johnson, A. D. Becke, C. D. Sherrill, and G. A. DiLabio, "Oscillations in meta-generalized-gradient approximation potential energy surfaces for dispersion-bound complexes," *The Journal of Chemical Physics* **131**, 034111 (2009).
- <sup>62</sup>C. A. Jiménez-Hoyos, B. G. Janesko, and G. E. Scuseria, "Evaluation of range-separated hybrid density functionals for the prediction of vibrational frequencies, infrared intensities, and Raman activities," *Physical Chemistry Chemical Physics* **10**, 6621–6629 (2008).
- <sup>63</sup>G. I. Csonka, A. D. French, G. P. Johnson, and C. A. Stortz, "Evaluation of Density Functionals and Basis Sets for Carbohydrates," *Journal of Chemical Theory and Computation* **5**, 679–692 (2009).
- <sup>64</sup>S. E. Wheeler and K. N. Houk, "Integration Grid Errors for Meta-GGA-Predicted Reaction Energies: Origin of Grid Errors for the M06 Suite of Functionals," *Journal of Chemical Theory and Computation* **6**, 395–404 (2010).
- <sup>65</sup>S. Dasgupta and J. M. Herbert, "Standard grids for high-precision integration of modern density functionals: SG-2 and SG-3," *Journal of Computational Chemistry* **38**, 869–882 (2017).
- <sup>66</sup>P. Morgante and R. Peverati, "The devil in the details: A tutorial review on some undervalued aspects of density functional theory calculations," *International Journal of Quantum Chemistry* **120**, e26332 (2020).
- <sup>67</sup>N. Mardirossian and M. Head-Gordon, "How Accurate Are the Minnesota Density Functionals for Noncovalent Interactions, Isomerization Energies, Thermochemistry, and Barrier Heights Involving Molecules Composed of Main-Group Elements?" *Journal of Chemical Theory and Computation* **12**, 4303–4325 (2016).
- <sup>68</sup>T. Gould, E. R. Johnson, and S. A. Tawfik, "Are dispersion corrections accurate outside equilibrium? A case study on benzene," *Beilstein Journal of Organic Chemistry* **14**, 1181–1191 (2018).
- <sup>69</sup>P. Hohenberg and W. Kohn, "Inhomogeneous Electron Gas," *Physical Review* **136**, B864–B871 (1964).
- <sup>70</sup>W. Kohn and L. J. Sham, "Self-Consistent Equations Including Exchange and Correlation Effects," *Physical Review* **140**, A1133–A1138 (1965).
- <sup>71</sup>J. P. Perdew, K. Burke, and M. Ernzerhof, "Generalized Gradient Approximation Made Simple," *Physical Review Letters* **77**, 3865–3868 (1996).
- <sup>72</sup>J. P. Perdew, K. Burke, and M. Ernzerhof, "Generalized Gradient Approximation Made Simple [Phys. Rev. Lett. 77, 3865 (1996)]," *Physical Review Letters* **78**, 1396–1396 (1997).
- <sup>73</sup>A. D. Becke, "On the large-gradient behavior of the density functional exchange energy," *The Journal of Chemical Physics* **85**, 7184–7187 (1986).
- <sup>74</sup>N. Mardirossian and M. Head-Gordon, "Mapping the genome of meta-generalized gradient approximation density functionals: The search for B97M-V," *The Journal of Chemical Physics* **142**, 074111 (2015).
- <sup>75</sup>C. Adamo and V. Barone, "Toward reliable density functional methods without adjustable parameters: The PBE0 model," *The Journal of Chemical Physics* **110**, 6158–6170 (1999).
- <sup>76</sup>A. D. Becke, "Density-functional thermochemistry. V. Systematic optimization of exchange-correlation functionals," *The Journal of Chemical Physics* **107**, 8554–8560 (1997).
- <sup>77</sup>J.-D. Chai and M. Head-Gordon, "Systematic optimization of long-range corrected hybrid density functionals," *The Journal of Chemical Physics* **128**, 084106 (2008).
- <sup>78</sup>N. Mardirossian and M. Head-Gordon, "ωB97X-V: A 10-parameter, range-separated hybrid, generalized gradient approximation density functional with nonlocal correlation, designed by a survival-of-the-fittest strategy," *Physical Chemistry Chemical Physics* **16**, 9904–9924 (2014).
- <sup>79</sup>N. Mardirossian and M. Head-Gordon, "ωB97M-V: A combinatorially optimized, range-separated hybrid, meta-GGA density functional with VV10 nonlocal correlation," *The Journal of Chemical Physics* **144**, 214110 (2016).
- <sup>80</sup>S. Grimme, "Semiempirical hybrid density functional with perturbative second-order correlation," *The Journal of Chemical Physics* **124**, 034108 (2006).
- <sup>81</sup>L. Goerigk and S. Grimme, "Efficient and Accurate Double-Hybrid-Meta-GGA Density Functionals—Evaluation with the Extended GMTKN30 Database for General Main Group Thermochemistry, Kinetics, and Noncovalent Interactions," *Journal of Chemical Theory and Computation* **7**,



291–309 (2011).

<sup>82</sup>N. Mardirossian and M. Head-Gordon, “Survival of the most transferable at the top of Jacob’s ladder: Defining and testing the  $\omega$ B97M(2) double hybrid density functional,” *The Journal of Chemical Physics* **148**, 241736 (2018).

<sup>83</sup>L. Goerigk, A. Hansen, C. Bauer, S. Ehrlich, A. Najibi, and S. Grimme, “A look at the density functional theory zoo with the advanced GMTKN55 database for general main group thermochemistry, kinetics and noncovalent interactions,” *Physical Chemistry Chemical Physics* **19**, 32184–32215 (2017).

<sup>84</sup>S. Grimme, S. Ehrlich, and L. Goerigk, “Effect of the damping function in dispersion corrected density functional theory,” *Journal of Computational Chemistry* **32**, 1456–1465 (2011).

<sup>85</sup>J.-D. Chai and M. Head-Gordon, “Long-range corrected hybrid density functionals with damped atom–atom dispersion corrections,” *Physical Chemistry Chemical Physics* **10**, 6615–6620 (2008).

<sup>86</sup>E. R. Johnson and A. D. Becke, “A post-Hartree-Fock model of intermolecular interactions: Inclusion of higher-order corrections,” *The Journal of Chemical Physics* **124**, 174104 (2006).

<sup>87</sup>A. Tkatchenko and M. Scheffler, “Accurate Molecular Van Der Waals Interactions from Ground-State Electron Density and Free-Atom Reference Data,” *Physical Review Letters* **102**, 073005 (2009).

<sup>88</sup>A. Tkatchenko, R. A. DiStasio, R. Car, and M. Scheffler, “Accurate and Efficient Method for Many-Body van der Waals Interactions,” *Physical Review Letters* **108**, 236402 (2012).

<sup>89</sup>Q. Wu and W. Yang, “Empirical correction to density functional theory for van der Waals interactions,” *The Journal of Chemical Physics* **116**, 515–524 (2002).

<sup>90</sup>E. R. Johnson, “Chapter 5 - The Exchange-Hole Dipole Moment Dispersion Model,” in *Non-Covalent Interactions in Quantum Chemistry and Physics*, edited

by A. Otero de la Roza and G. A. DiLabio (Elsevier, 2017) pp. 169–194.

<sup>91</sup>A. J. A. Price, K. R. Bryenton, and E. R. Johnson, “Requirements for an accurate dispersion-corrected density functional,” *The Journal of Chemical Physics* **154**, 230902 (2021).

<sup>92</sup>T. Schwabe and S. Grimme, “Double-hybrid density functionals with long-range dispersion corrections: Higher accuracy and extended applicability,” *Physical Chemistry Chemical Physics* **9**, 3397–3406 (2007).

<sup>93</sup>A. D. Becke, “A multicenter numerical integration scheme for polyatomic molecules,” *The Journal of Chemical Physics* **88**, 2547–2553 (1988).

<sup>94</sup>H. Laqua, J. Kussmann, and C. Ochsenfeld, “An improved molecular partitioning scheme for numerical quadratures in density functional theory,” *The Journal of Chemical Physics* **149**, 204111 (2018).

<sup>95</sup>O. Treutler and R. Ahlrichs, “Efficient molecular numerical integration schemes,” *The Journal of Chemical Physics* **102**, 346–354 (1995).

<sup>96</sup>V. Lebedev and D. Laikov, “A QUADRATURE FORMULA FOR THE SPHERE OF THE 131ST ALGEBRAIC ORDER OF ACCURACY,” *Doklady Mathematics* (1999).

<sup>97</sup>K. Sorathia, D. Frantzov, and D. P. Tew, “Improved CPS and CBS Extrapolation of PNO-CCSD(T) Energies: The MOBH35 and ISOL24 Data Sets,” *Journal of Chemical Theory and Computation* **20**, 2740–2750 (2024).

<sup>98</sup>G. Schmitz and C. Hättig, “Perturbative triples correction for local pair natural orbital based explicitly correlated CCSD(F12\*) using Laplace transformation techniques,” *The Journal of Chemical Physics* **145**, 234107 (2016).

<sup>99</sup>K. R. Bryenton, A. A. Adeleke, S. G. Dale, and E. R. Johnson, “Delocalization error: The greatest outstanding challenge in density-functional theory,” *WIREs Computational Molecular Science* **13**, e1631 (2023).

<sup>100</sup>F. O. Kannemann, *Development And Benchmarking Of A Semilocal Density-Functional* Ph.D. thesis, Department of Chemistry, Dalhousie University (2013).

<sup>101</sup>A. D. Becke, “Real-space post-Hartree-Fock correlation models,” *The Journal of Chemical Physics* **122**, 064101 (2005).

# Supplementary Information: Endofullerenes and Dispersion-Corrected Density Functional Approximations: A Cautionary Tale

K. Panchagnula\*<sup>1</sup>, D. Graf<sup>2</sup>, K.R. Bryenton<sup>3</sup>, E.R. Johnson<sup>1,3,4</sup> and A.J.W. Thom<sup>1</sup>

<sup>1</sup>*Yusuf Hamied Department of Chemistry, University of Cambridge, Cambridge, United Kingdom*

<sup>2</sup>*Department of Chemistry, University of Munich (LMU), Munich, Germany*

<sup>3</sup>*Department of Physics and Atmospheric Science, Dalhousie University, 6310 Coburg Road, Halifax, Nova Scotia, Canada*

<sup>4</sup>*Department of Chemistry, Dalhousie University, 6243 Alumni Crescent, Halifax, Nova Scotia, Canada*

(\*Electronic mail: ksp31@cam.ac.uk)

(Dated: 4 March 2025)

## SI 1. COMPUTATIONAL DETAILS

### A. FermiONs++ Details

All the calculations using the PBE,<sup>1,2</sup> B97M-V,<sup>3</sup> B97,<sup>4</sup>  $\omega$ -B97,<sup>5</sup>  $\omega$ -B97X,<sup>5</sup>  $\omega$ -B97X-V,<sup>6</sup>  $\omega$ -B97M-V,<sup>7</sup> B2PLYP,<sup>8</sup> and PWPB95<sup>9</sup> functionals were carried out using the FermiONs++ program package<sup>10,11</sup> developed in the Ochsenfeld group. Calculations employing functionals up to rung 4 were carried out using the def2-TZVPPD<sup>12,13</sup> basis set together with the def2-TZVPP-RI-JK basis set for resolution of the identity Coulomb (RI-J) builds.<sup>14</sup> For rung 5 functionals the def2-QZVP<sup>15</sup> basis set together with the def2-TZVP-RI<sup>16,17</sup> basis set for the RI-MP2 part was employed; the basis set for RI-J was unchanged. All calculations were considered converged when the energy difference decreased below  $1.0 \times 10^{-8}$  and the norm of the commutator  $[\mathbf{F}, \mathbf{P}]$  was smaller than  $1.0 \times 10^{-7}$ . For the grid generation, we employed the partitioning scheme described in Ref. 18. The radial grids were constructed using the M4 mapping described in Ref. 19. For the angular grids, we employed Lebedev-Laikov grids.<sup>20</sup>

Each atomic grid is generally constructed as a product of radial ( $\tau$ ) and angular ( $\sigma$ ) grids, expressed as

$$\mathbf{r}_{\text{atomic}} = r_{\tau} \mathbf{r}_{\sigma} \quad (\text{SI } 1)$$

$$\omega_{\text{atomic}} = \omega_{\tau} \omega_{\sigma} \quad (\text{SI } 2)$$

Here,  $r_{\tau}$  denotes the radius of the radial shell,  $\mathbf{r}_{\sigma}$  specifies the position of the angular grid point on the unit sphere,  $\omega_{\tau}$  denotes the radial grid weight, and  $\omega_{\sigma}$  represents the angular grid weight. Due to the increase in isotropy of the density moving towards the nuclei, the atomic grid is partitioned into three regions

$$\tau_{\text{inner}} \leq \frac{n_{\text{rad}}}{3} \quad (\text{SI } 3)$$

$$\frac{n_{\text{rad}}}{3} < \tau_{\text{middle}} \leq \frac{n_{\text{rad}}}{2} \quad (\text{SI } 4)$$

$$\tau_{\text{outer}} > \frac{n_{\text{rad}}}{2} \quad (\text{SI } 5)$$

with the number of angular grid points increasing from inner to middle to outer. Furthermore, the number of radial points is increased for heavier elements. For more details and the exact specifications of the grids (denoted g1 to g7), the reader

is referred to Ref. 18. To evaluate the VV10 correction,<sup>21</sup> the g7 grid was employed in all calculations. For the seminumerical evaluation of exact exchange,<sup>22,23</sup> we always employed the multi-grid denoted as gm7. For the XC functionals shown in Figure 1b of the main text, all used a (200 radial, 1454 angular) integration grid to ensure numerical stability. Convergence testing of the  $\omega$ -B97M-V PES slice with respect to both angular and radial grid sizes is shown in Fig. SI 1.

### B. ORCA Computational Details

The calculations using the  $\omega$ -B97M(2)<sup>24</sup> functional were carried out with the ORCA software package.<sup>25–29</sup> The calculations employed the def2-QZVP basis set, together with the def2/J basis set for RI-J and def2-TZVPPD/C basis set for the RI-MP2 part. For the SCF, very tight settings were chosen (keyword VERYTIGHT). The grids were built using the DEFGRID3 keyword. The VV10 correction was evaluated self-consistently (keyword SCNL).

### C. CCSD(T0) Computational Details

The CCSD(T0) calculations are paired natural orbital (PNO) calculations, extrapolated to the complete PNO space (CPS) and complete basis set (CBS) limits from double- $\zeta$  and triple- $\zeta$  calculations, with counterpoise correction, calculated using TURBOMOLE.<sup>30,31</sup> A single point quadruple- $\zeta$  calculation runs for 5 days on 1 node, 48 cores requiring 200GB RAM and 2TB disk. Perturbative triples and the counterpoise correction are significant contributions, indicating tight PNO thresholds and large basis sets are required to achieve wavenumber accuracy.

### D. FHI-aims Computational Details

The FHI-aims calculations were carried out using version 240920-1 of the code.<sup>32</sup> The calculations made use of FHI-aims' hybrid DFT framework<sup>33–35</sup>, through its ELSI infrastructure<sup>36</sup>, real-space partitioning and parallelization<sup>37</sup>, and efficient resolution of identity (RI) approach<sup>38</sup> for linear scaling. The default tight basis settings were used, which

are approximately equivalent in accuracy to the Gaussian cc-PVQZ basis set. Finer radial grids than the `tight` defaults were necessary in order to achieve a wavenumber-level of accuracy and eliminate PES oscillations from hybrids with high levels of Hartree-Fock exchange mixing. Convergence testing showed that a radial grid of 100 points was sufficient, set via keywords `radial_base 50.0 7.0` combined with `radial_multiplier 2.0`.

In the present work, dispersion corrections were paired with the generalized gradient approximation (GGA) functionals: PBE and B86bPBE; and their associated hybrid counterparts: PBE0 and B86bPBE0. The PBE functional was selected due to its widespread use in the literature, while B86bPBE was selected as it is our preferred GGA functional for its ability to accurately describe non-bonded repulsion, as a result of the adherence of its enhancement factor to the appropriate large reduced-density-gradient limit.<sup>39</sup>

The PBE0 and B86bPBE0 hybrid exchange-correlation functionals have the form

$$E_{XC} = (1 - a_X)E_X + a_X E_X^{\text{HF}} + E_C^{\text{PBE}}, \quad (\text{SI } 6)$$

where  $E_X$  represents either the PBE or B86b exchange energy,  $E_X^{\text{HF}}$  is the exact (Hartree-Fock) exchange energy,  $E_C^{\text{PBE}}$  is the PBE correlation energy, and  $a_X$  is the exact-exchange mixing coefficient. By default, both PBE0 and B86bPBE0 use  $a_X = 0.25$ , which corresponds to using a mixture of 75% GGA and 25% HF exchange energies. These two hybrid functionals were used to investigate how the barrier height (BH) and minima positions ( $z_m$ ) of the Ne@C<sub>70</sub> system was impacted by varying the exact exchange mixing parameter,  $a_X$ . For the PBE0 functional, this was achievable by selecting `xc pbe0` in FHI-aim’s `control.in` file, then adjusting the exact exchange mixing parameter via the `hybrid_xc_coeff` keyword. We have implemented the B86bPBE0 functional to work similarly, and it may be called using `xc b86bpbe0`.

The XDM model calculates the dispersion energy via an asymptotic pairwise sum as

$$E_{\text{disp}}^{\text{XDM}} = - \sum_{i < j} \frac{f_6^{\text{BJ}} C_{6,ij}}{R_{ij}^6} + \frac{f_8^{\text{BJ}} C_{8,ij}}{R_{ij}^8} + \frac{f_{10}^{\text{BJ}} C_{10,ij}}{R_{ij}^{10}}, \quad (\text{SI } 7)$$

where  $C_{n,ij}$  are the interatomic dispersion coefficients for atoms  $i$  and  $j$ .  $C_6$  captures instantaneous dipole-dipole interactions,  $C_8$  captures dipole-quadrupole interactions, and  $C_{10}$  captures both dipole-octupole and quadrupole-quadrupole interactions. To prevent unphysical divergence of the dispersion energy at short internuclear separations, the use of damping functions is required. Here,

$$f_n^{\text{BJ}}(R_{ij}) = \frac{R_{ij}^n}{R_{ij}^n + R_{\text{vdw},ij}^n}, \quad (\text{SI } 8)$$

is the Becke-Johnson damping function<sup>40</sup>, where

$$R_{\text{vdw},ij} = a_1 R_{c,ij} + a_2, \quad (\text{SI } 9)$$

is the van der Waals radius, defined in terms of  $R_{c,ij}$  — the “critical” separation where successive dispersion coefficients

TABLE SI 1: Optimal XDM Becke-Johnson damping parameters  $a_1$  and  $a_2$  (in Å) for the PBE0 and B86bPBE0 hybrid functionals with varied exact-exchange mixing coefficients ( $a_X$ ). Calculations used FHI-aims version 240920-1 with `tight` basis defaults. The mean absolute errors (MAE, in kcal/mol) for the KB49 fit set are also shown.

$a_X$	PBE0 / <code>tight</code>			B86bPBE0 / <code>tight</code>		
	$a_1$	$a_2$ (Å)	MAE	$a_1$	$a_2$ (Å)	MAE
0.00	0.5124	2.2588	0.49	0.9004	0.7808	0.39
0.05	0.5044	2.2804	0.46	0.8639	0.9037	0.36
0.10	0.4963	2.3037	0.43	0.8280	1.0267	0.34
0.15	0.4882	2.3287	0.42	0.7932	1.1473	0.33
0.20	0.4799	2.3559	0.41	0.7600	1.2645	0.32
0.25	0.4713	2.3855	0.40	0.7284	1.3780	0.32
0.30	0.4626	2.4169	0.40	0.6986	1.4876	0.32
0.35	0.4535	2.4512	0.40	0.6701	1.5943	0.33
0.40	0.4440	2.4878	0.40	0.6429	1.6986	0.33
0.45	0.4339	2.5280	0.40	0.6166	1.8018	0.34
0.50	0.4233	2.5711	0.41	0.5910	1.9041	0.36
0.60	0.3999	2.6686	0.44	0.5395	2.1147	0.40
0.70	0.3728	2.7831	0.48	0.4842	2.3442	0.44
0.80	0.3386	2.9260	0.53	0.4211	2.6049	0.51
0.90	0.2966	3.0994	0.57	0.3429	2.9217	0.58
1.00	0.2432	3.3152	0.65	0.2425	3.3177	0.65

become equal. The empirical parameters,  $a_1$  and  $a_2$ , are optimized by minimizing the root-mean-square-percent error (RMSPE) on the KB49 benchmark<sup>41</sup> of small molecular dimers for each basis set and functional combination.

Since XDM is fitted to each functional and basis combination, the  $a_1$  and  $a_2$  damping coefficients needed to be re-optimized for each value of  $a_X$  considered. A table of optimally fitted XDM damping coefficients and corresponding mean absolute errors (MAEs) on the KB49 benchmark are presented in Table SI 1. Values are reported for the PBE0- and B86bPBE0-based hybrid functionals for each value of  $a_X$  considered, all using the `tight` basis set. We have used values for  $a_X \leq 0.5$  but not higher, as values above 50% are not typically considered as they become increasingly poor for thermochemistry.

When XDM (or any DC) is optimized using a benchmark that includes molecular dimers, the damping parameters partially correct basis-set incompleteness and errors in the base XC functional’s prediction of non-bonded repulsion or short-range dispersion-like binding. Thus, “ideal” parameters can be obtained by considering only noble gas dimer interactions at the CBS limit with a dispersionless base functional; this parameterization is denoted as XDM(BJ<sub>NG</sub>) in this work. Minimizing the RMSPD for six noble gas diatomics (combinations of He, Ne, and Ar) at the CP-corrected PW86bPBE-XDM/aug-pV5Z level of theory yields BJ damping parameters of  $a_1 = 0.65$  and  $a_2 = 1.68$  Å.<sup>42</sup>

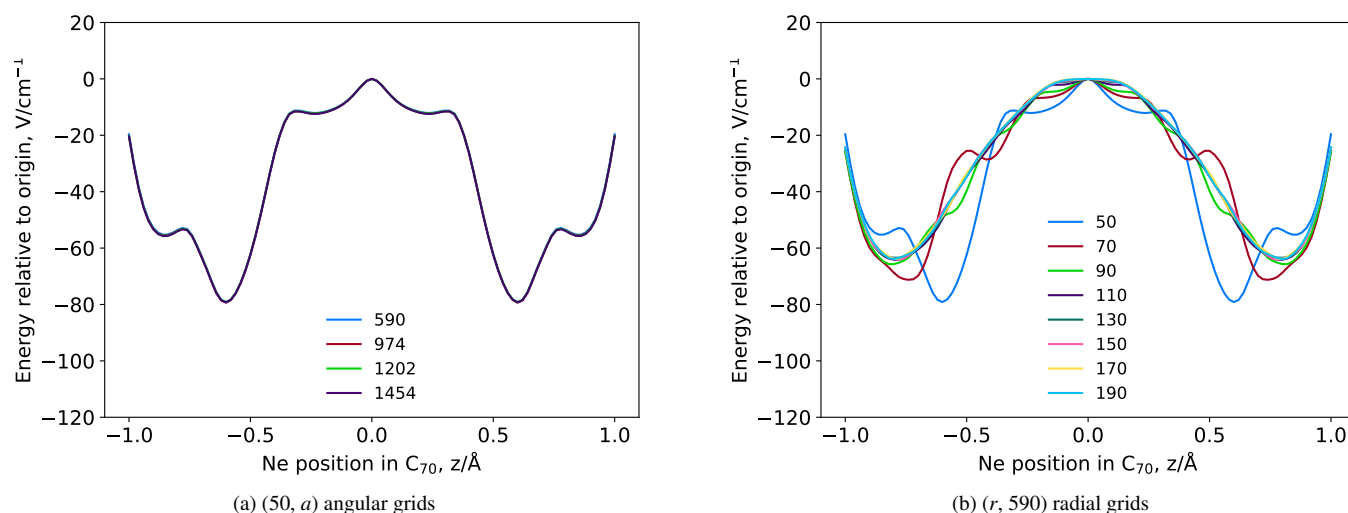


FIG. SI 1: Effects of varying (a) angular and (b) radial grid sizes on the oscillatory behaviour of the PES for the  $\omega$ -B97M-V functional. Angular grids are (50, [590, 974, 1202, 1454]) in blue, maroon, light green and purple; Radial grids are ([50, 70, 90, 110, 130, 150, 170, 190], 590) in blue, maroon, light green, purple, forest green, pink, yellow and light blue.

## SI 2. META-GGA OSCILLATIONS

For the  $\omega$ -B97M-V functional, one-dimensional slices of the Ne@C<sub>70</sub> PES are presented in Figure SI 1, with Figure SI 1a varying the angular grid size from 590 to 974, 1202, and 1454 grid points, each with 50 radial points. As the curves are almost completely overlapping, it is evident that the 590 Lebedev grid is sufficient for the numerical quadrature. However, the curve shape demonstrates severe oscillatory behaviour, as has been commonly seen in the literature with mGGA functionals.<sup>40,43</sup> Figure SI 1b shows analogous results where the angular grid is fixed at 590 points and the radial grid size varied from 50 to 190 in increments of 20 points. As the quadrature is steadily increased, the region near the origin smoothens and flattens, with the minima around  $\pm 0.75\text{\AA}$  revealing themselves. The smallest grid to give an acceptable PES is the (150, 590) mesh, but this may not be constant for all functionals.

## SI 3. IMPACT OF VARYING EXACT-EXCHANGE MIXING IN HYBRID FUNCTIONALS

Plots of the PESs obtained with XDM-corrected hybrid functionals, from which the BHs and  $z_m$ s given in Figure 3 were extracted, are shown in Figure SI 2. The HF exact exchange proportion is varied between [0,50]% in increments of 5% from violet to red. As seen in Figure SI 2, increasing the amount of exact HF exchange results in a transition from a single-well potential to a double well. The introduction of inflection points in the potential, although much less dramatic than the oscillatory behaviour observed in Figure SI 1, is also noticeable upon the increasing the exact-exchange mixing. The precise interval of the optimal exact-exchange

percentage may be dependent on both the DFA, and the dispersion correction used.

- <sup>1</sup>J. P. Perdew, K. Burke, and M. Ernzerhof, "Generalized Gradient Approximation Made Simple," *Physical Review Letters* **77**, 3865–3868 (1996).
- <sup>2</sup>J. P. Perdew, K. Burke, and M. Ernzerhof, "Generalized Gradient Approximation Made Simple [Phys. Rev. Lett. 77, 3865 (1996)]," *Physical Review Letters* **78**, 1396–1396 (1997).
- <sup>3</sup>N. Mardirossian and M. Head-Gordon, "Mapping the genome of meta-generalized gradient approximation density functionals: The search for B97M-V," *The Journal of Chemical Physics* **142**, 074111 (2015).
- <sup>4</sup>A. D. Becke, "Density-functional thermochemistry. V. Systematic optimization of exchange-correlation functionals," *The Journal of Chemical Physics* **107**, 8554–8560 (1997).
- <sup>5</sup>J.-D. Chai and M. Head-Gordon, "Systematic optimization of long-range corrected hybrid density functionals," *The Journal of Chemical Physics* **128**, 084106 (2008).
- <sup>6</sup>N. Mardirossian and M. Head-Gordon, " $\omega$ B97X-V: A 10-parameter, range-separated hybrid, generalized gradient approximation density functional with nonlocal correlation, designed by a survival-of-the-fittest strategy," *Physical Chemistry Chemical Physics* **16**, 9904–9924 (2014).
- <sup>7</sup>N. Mardirossian and M. Head-Gordon, " $\omega$ B97M-V: A combinatorially optimized, range-separated hybrid, meta-GGA density functional with VV10 nonlocal correlation," *The Journal of Chemical Physics* **144**, 214110 (2016).
- <sup>8</sup>S. Grimme, "Semiempirical hybrid density functional with perturbative second-order correlation," *The Journal of Chemical Physics* **124**, 034108 (2006).
- <sup>9</sup>L. Goerigk and S. Grimme, "Efficient and Accurate Double-Hybrid-Meta-GGA Density Functionals—Evaluation with the Extended GMTKN30 Database for General Main Group Thermochemistry, Kinetics, and Noncovalent Interactions," *Journal of Chemical Theory and Computation* **7**, 291–309 (2011).
- <sup>10</sup>J. Kussmann and C. Ochsenfeld, "Pre-selective screening for matrix elements in linear-scaling exact exchange calculations," *The Journal of Chemical Physics* **138**, 134114 (2013).
- <sup>11</sup>J. Kussmann and C. Ochsenfeld, "Preselective Screening for Linear-Scaling Exact Exchange-Gradient Calculations for Graphics Processing Units and General Strong-Scaling Massively Parallel Calculations," *Journal of Chemical Theory and Computation* **11**, 918–922 (2015).

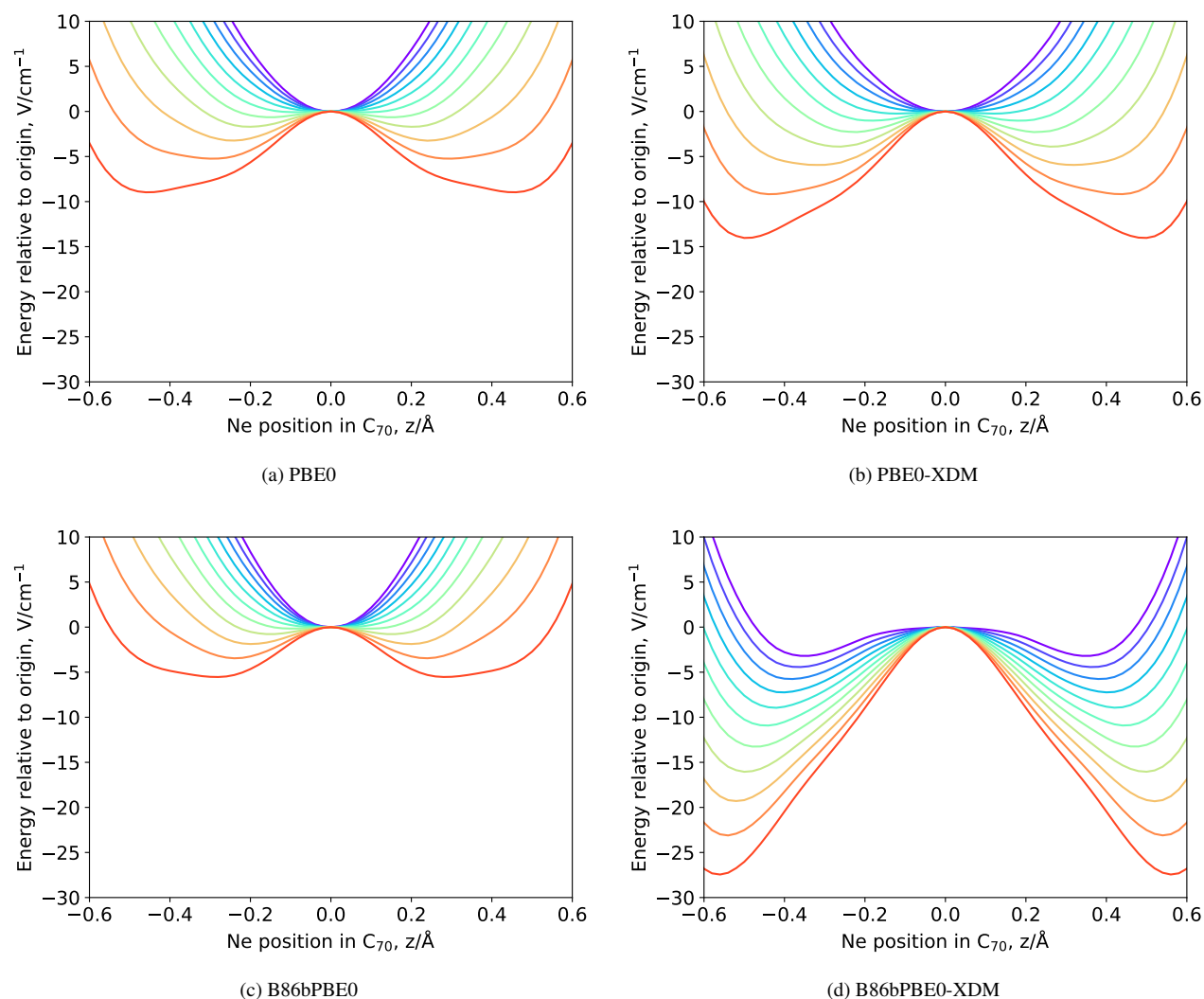


FIG. SI 2: PES slices for varying HF exchange proportion from 0% (violet) to 50% (red) in increments of 5% for (a) PBE0, (b) PBE0-XDM, (c) B86bPBE0, and (d) B86bPBE0-XDM for points separated by 0.02Å. These curves correspond to the features plotted in Figure 3 of the main text.

<sup>12</sup>D. Rappoport and F. Furche, “Property-optimized Gaussian basis sets for molecular response calculations,” *The Journal of Chemical Physics* **133**, 134105 (2010).

<sup>13</sup>F. Weigend and R. Ahlrichs, “Balanced basis sets of split valence, triple zeta valence and quadruple zeta valence quality for H to Rn: Design and assessment of accuracy,” *Physical Chemistry Chemical Physics* **7**, 3297–3305 (2005).

<sup>14</sup>J. Kussmann, H. Laqua, and C. Ochsenfeld, “Highly Efficient Resolution-of-Identity Density Functional Theory Calculations on Central and Graphics Processing Units,” *Journal of Chemical Theory and Computation* **17**, 1512–1521 (2021).

<sup>15</sup>F. Weigend, F. Furche, and R. Ahlrichs, “Gaussian basis sets of quadruple zeta valence quality for atoms H–Kr,” *The Journal of Chemical Physics* **119**, 12753–12762 (2003).

<sup>16</sup>F. Weigend, M. Häser, H. Patzelt, and R. Ahlrichs, “RI-MP2: Optimized auxiliary basis sets and demonstration of efficiency,” *Chemical Physics Letters* **294**, 143–152 (1998).

<sup>17</sup>C. Hättig, “Optimization of auxiliary basis sets for RI-MP2 and RI-CC2 calculations: Core–valence and quintuple- $\zeta$  basis sets for H to Ar and QZVPP basis sets for Li to Kr,” *Physical Chemistry Chemical Physics* **7**, 59–66

(2005).

<sup>18</sup>H. Laqua, J. Kussmann, and C. Ochsenfeld, “An improved molecular partitioning scheme for numerical quadratures in density functional theory,” *The Journal of Chemical Physics* **149**, 204111 (2018).

<sup>19</sup>O. Treutler and R. Ahlrichs, “Efficient molecular numerical integration schemes,” *The Journal of Chemical Physics* **102**, 346–354 (1995).

<sup>20</sup>V. Lebedev and D. Laikov, “A QUADRATURE FORMULA FOR THE SPHERE OF THE 131ST ALGEBRAIC ORDER OF ACCURACY,” *Doklady Mathematics* (1999).

<sup>21</sup>O. A. Vydrov and T. Van Voorhis, “Nonlocal van der Waals density functional: The simpler the better,” *The Journal of Chemical Physics* **133**, 244103 (2010).

<sup>22</sup>H. Laqua, J. Kussmann, and C. Ochsenfeld, “Efficient and Linear-Scaling Seminumerical Method for Local Hybrid Density Functionals,” *Journal of Chemical Theory and Computation* **14**, 3451–3458 (2018).

<sup>23</sup>H. Laqua, T. H. Thompson, J. Kussmann, and C. Ochsenfeld, “Highly Efficient, Linear-Scaling Seminumerical Exact-Exchange Method for Graphic Processing Units,” *Journal of Chemical Theory and Computation* **16**, 1456–1468 (2020).

- <sup>24</sup>N. Mardirossian and M. Head-Gordon, "Survival of the most transferable at the top of Jacob's ladder: Defining and testing the  $\omega$ B97M(2) double hybrid density functional," *The Journal of Chemical Physics* **148**, 241736 (2018).
- <sup>25</sup>F. Neese, F. Wennmohs, U. Becker, and C. Riplinger, "The ORCA quantum chemistry program package," *The Journal of Chemical Physics* **152**, 224108 (2020).
- <sup>26</sup>F. Neese, "Software update: The ORCA program system—Version 5.0," *WIREs Computational Molecular Science* **12**, e1606 (2022).
- <sup>27</sup>C. Kollmar, K. Sivalingham, B. Helmich-Paris, C. Angeli, and F. Neese, "A perturbation-based super-CI approach for the orbital optimization of a CASSCF wave function," *Journal of Computational Chemistry* **40**, 1463–1470 (2019).
- <sup>28</sup>F. Neese, "The SHARK integral generation and digestion system," *Journal of Computational Chemistry* **44**, 381–396 (2023).
- <sup>29</sup>M. Ugandi and M. Roemelt, "A recursive formulation of one-electron coupling coefficients for spin-adapted configuration interaction calculations featuring many unpaired electrons," *International Journal of Quantum Chemistry* **123**, e27045 (2023).
- <sup>30</sup>Y. J. Franzke, C. Holzer, J. H. Andersen, T. Begušić, F. Bruder, S. Coriani, F. Della Sala, E. Fabiano, D. A. Fedotov, S. Fürst, S. Gillhuber, R. Grotjahn, M. Kaupp, M. Kehry, M. Krstić, F. Mack, S. Majumdar, B. D. Nguyen, S. M. Parker, F. Pauly, A. Pausch, E. Perlt, G. S. Phun, A. Rajabi, D. Rappoport, B. Samal, T. Schrader, M. Sharma, E. Tapavicza, R. S. Treß, V. Voora, A. Wodyński, J. M. Yu, B. Zerulla, F. Furche, C. Hättig, M. Sierka, D. P. Tew, and F. Weigend, "TURBOMOLE: Today and Tomorrow," *Journal of Chemical Theory and Computation* **19**, 6859–6890 (2023).
- <sup>31</sup>S. G. Balasubramani, G. P. Chen, S. Coriani, M. Diedenhofen, M. S. Frank, Y. J. Franzke, F. Furche, R. Grotjahn, M. E. Harding, C. Hättig, A. Hellweg, B. Helmich-Paris, C. Holzer, U. Huniar, M. Kaupp, A. Marefat Khah, S. Karbalaee Khani, T. Müller, F. Mack, B. D. Nguyen, S. M. Parker, E. Perlt, D. Rappoport, K. Reiter, S. Roy, M. Rückert, G. Schmitz, M. Sierka, E. Tapavicza, D. P. Tew, C. van Wüllen, V. K. Voora, F. Weigend, A. Wodyński, and J. M. Yu, "TURBOMOLE: Modular program suite for ab initio quantum-chemical and condensed-matter simulations," *The Journal of Chemical Physics* **152**, 184107 (2020).
- <sup>32</sup>V. Blum, R. Gehrke, F. Hanke, P. Havu, V. Havu, X. Ren, K. Reuter, and M. Scheffler, "Ab Initio molecular simulations with numeric atom-centered orbitals," *Computer Physics Communications* **180**, 2175–2196 (2009).
- <sup>33</sup>X. Ren, P. Rinke, V. Blum, J. Wieferink, A. Tkatchenko, A. Sanfilippo, K. Reuter, and M. Scheffler, "Resolution-of-identity approach to Hartree–Fock, hybrid density functionals, RPA, MP2 and GW with numeric atom-centered orbital basis functions," *New Journal of Physics* **14**, 053020 (2012).
- <sup>34</sup>S. V. Levchenko, X. Ren, J. Wieferink, R. Johanni, P. Rinke, V. Blum, and M. Scheffler, "Hybrid functionals for large periodic systems in an all-electron, numeric atom-centered basis framework," *Computer Physics Communications* **192**, 60–69 (2015).
- <sup>35</sup>S. Kokott, F. Merz, Y. Yao, C. Carbogno, M. Rossi, V. Havu, M. Rampp, M. Scheffler, and V. Blum, "Efficient all-electron hybrid density functionals for atomistic simulations beyond 10 000 atoms," *The Journal of Chemical Physics* **161**, 024112 (2024).
- <sup>36</sup>V. W.-z. Yu, F. Corsetti, A. García, W. P. Huhn, M. Jacquelin, W. Jia, B. Lange, L. Lin, J. Lu, W. Mi, A. Seifitokaldani, Á. Vázquez-Mayagoitia, C. Yang, H. Yang, and V. Blum, "ELSI: A unified software interface for Kohn–Sham electronic structure solvers," *Computer Physics Communications* **222**, 267–285 (2018).
- <sup>37</sup>V. Havu, V. Blum, P. Havu, and M. Scheffler, "Efficient  $O(N)$  integration for all-electron electronic structure calculation using numeric basis functions," *Journal of Computational Physics* **228**, 8367–8379 (2009).
- <sup>38</sup>A. C. Ihrig, J. Wieferink, I. Y. Zhang, M. Ropo, X. Ren, P. Rinke, M. Scheffler, and V. Blum, "Accurate localized resolution of identity approach for linear-scaling hybrid density functionals and for many-body perturbation theory," *New Journal of Physics* **17**, 093020 (2015).
- <sup>39</sup>A. J. A. Price, K. R. Bryenton, and E. R. Johnson, "Requirements for an accurate dispersion-corrected density functional," *The Journal of Chemical Physics* **154**, 230902 (2021).
- <sup>40</sup>E. R. Johnson and A. D. Becke, "A post-Hartree–Fock model of intermolecular interactions," *The Journal of Chemical Physics* **123**, 024101 (2005).
- <sup>41</sup>F. O. Kannemann and A. D. Becke, "Van der Waals Interactions in Density-Functional Theory: Intermolecular Complexes," *Journal of Chemical Theory and Computation* **6**, 1081–1088 (2010).
- <sup>42</sup>F. O. Kannemann, *Development And Benchmarking Of A Semilocal Density-Functional* Ph.D. thesis, Department of Chemistry, Dalhousie University (2013).
- <sup>43</sup>E. R. Johnson, A. D. Becke, C. D. Sherrill, and G. A. DiLabio, "Oscillations in meta-generalized-gradient approximation potential energy surfaces for dispersion-bound complexes," *The Journal of Chemical Physics* **131**, 034111 (2009).